RSC Advances

PAPER

View Article Online
View Journal | View Issue

Cite this: *RSC Adv.*, 2017, **7**, 33994

Prussian blue derived iron oxide nanoparticles wrapped in graphene oxide sheets for electrochemical supercapacitors†

Shunsuke Tanaka,[ab] Rahul R. Salunkhe,[bc] Yusuf Valentino Kaneti,[b] Victor Malgras,[b] Saad M. Alshehri,[c] Tansir Ahamad,[c] Mohamed B. Zakaria,[b] Shi Xue Dou,[a] Yusuke Yamauchi*[abc] and Md. Shahriar A. Hossain*[ab]

Hybrid materials have shown promising potential for energy storage applications, such as supercapacitors due to the combined properties or advantages of two (or more) individual constituents. In this work, we report the fabrication of a new composite which combines graphene oxide (GO) sheets with Prussian blue (PB) nanoparticles, which act as a precursor for iron oxide (IO). The GO/PB composite precursors with different GO : PB ratios can be successfully converted into nanoporous GO/IO hybrid composites through a thermal treatment in air at 400 °C. In the resulting GO/IO composites, the GO sheets are efficiently spaced due to the insertion of IO layers. Interestingly, the GO/IO hybrid (GO : PB ratio = 25 : 75) exhibits a higher surface area of 120 $m^2 g^{-1}$ compared to pure GO (34.9 $m^2 g^{-1}$) and IO (93.1 $m^2 g^{-1}$) samples. When employed as a supercapacitor electrode, the GO/IO hybrid (prepared from GO : PB = 75 : 25) showed a higher specific capacitance of 91 F g^{-1} at a scan rate of 20 mV s^{-1}, compared to pure GO (81 F g^{-1}) and pure IO (47 F g^{-1}). The enhanced electrochemical performance of the GO/IO hybrid electrode may be attributed to the insertion of IO nanoparticles in between the GO layers which creates a well-spaced electrical transportation path for electrolytes and ions, whilst also enabling easy access for the electrolytes to the whole electrode surface. Furthermore, the presence of GO in the GO/IO hybrid composite helps to lower the resistivity of IO and increase the specific capacitance value of the hybrid, as a result of the improved conductivity.

Received 17th March 2017
Accepted 13th June 2017

DOI: 10.1039/c7ra03179c

rsc.li/rsc-advances

1. Introduction

Over the years, the fabrication of hybrid materials has attracted significant interest due to the possibilities of combining the properties or advantages of two (or more) individual constituents to meet the demand for specific applications.[1] For example, multi-layered hybrid structures with various compositions can be designed at the nanometer-level and used for a wide range of applications such as biomedical,[2] catalytic,[3] sensor[4] and energy storage applications.[5] They can be fabricated using a convenient layer-by-layer (LbL) approach, which is known to be a simple, inexpensive, and versatile process. This synthesis technique can be performed through various interactions, including electrostatic, hydrogen bonding, or charge-transfer, as well as through chemical reactions such as sol–gel, electrochemical coupling, or click reactions.[1] Recently, highly flexible two-dimensional (2D) graphene oxide (GO) sheets have gained increasing attention because of their potential applications.[6] In particular, the hybridization of GO sheets with various nanomaterials is a promising strategy because of the unique properties arising from the resulting composite.[7]

The accelerating surge in global energy consumption has prompted research to seek new and more efficient ways of converting and storing energy. Supercapacitors (SCs) (*i.e.*, electrochemical capacitors) are considered to be one of the most promising energy storage devices due to their fast energy delivery, short charging duration, high power density, long durability and environmental friendliness.[8] High surface area carbon materials[9] such as porous carbon, activated carbon, carbon nanofiber, carbon nanotubes, and graphene, are currently among the most widely investigated candidates for SC electrodes. 2D GO sheets have shown promising potential as SC electrodes, because of their relatively high conductivity and layered structures which may allow for easy transportation of electrolytes and ions. Unfortunately, they have a natural tendency to stack through van der Waals forces,[10] making it

[a]*Institute for Superconducting & Electronic Materials (ISEM), Australian Institute for Innovative Materials (AIIM), University of Wollongong, Squires Way, North Wollongong, NSW 2500, Australia. E-mail: yusuke@uow.edu.au; shahriar@uow.edu.au*

[b]*International Center for Materials Nanoarchitectonics (MANA), National Institute for Materials Science (NIMS), 1-1 Namiki, Tsukuba, Ibaraki 305-0044, Japan*

[c]*Department of Chemistry, College of Science, King Saud University, Riyadh 11451, Kingdom of Saudi Arabia*

† Electronic supplementary information (ESI) available. See DOI: 10.1039/c7ra03179c

difficult to efficiently utilize their whole surface area. Thus, achieving a good capacitive performance from pure GO remains a challenging task.

In recent years, the combination of GO with other materials to create GO-based hybrid materials has been considered as an effective method to prevent the stacking of GO during the synthesis process and to improve its properties in terms of conductivity and surface area.[11] Metal oxides are known to provide high energy densities for SC-based applications, because of their pseudocapacitance. Considerable efforts have been invested towards the investigations of metal oxides for SCs (*e.g.*, cobalt oxide,[12] nickel oxide,[13] copper oxide,[14] and iron oxide (IO)[15]). IOs have been considered as promising candidates as electrode materials for SCs due to their high abundance, environmental friendliness, low synthesis costs, and their high theoretical specific capacities.[16] In this study, we prepare a novel hybrid material combining GO sheets with Prussian blue nanoparticles which is further converted, through thermal treatment, into nanoporous GO/IO composite useful for SC applications.

2. Experimental

Chemicals and materials

Sodium hexacyanoferrate(II) decahydrate ($Na_4[Fe(CN)_6]\cdot 10H_2O$) and iron(III) chloride hexahydrate ($FeCl_3\cdot 6H_2O$) were purchased from Sigma-Aldrich, USA. Trisodium citrate dihydrate (TSCD), and sulfuric acid were purchased from Nacalai Tesque, Japan. Potassium hydroxide (KOH) and sodium nitrate ($NaNO_3$) were purchased from Wako, Japan. Nanographite platelets (N008-100-N) of 100 nm thickness were used as raw materials to prepare the graphene oxide (GO) sheets (Angestron materials Inc.). Potassium permanganate ($KMnO_4$) and hydrogen peroxide (H_2O_2) were purchased from Kanto Chemicals Co., Inc. All chemical reagents were used without further purification.

Synthesis of GO sheets

Graphene oxide was synthesized by the modified Hummer's method. Sodium nitrate (0.3 g) was firstly dissolved in sulfuric acid solution (10 mL) under constant stirring. Nanographite platelet powder was then added into the above solution and further stirred for 30 min. After that, $KMnO_4$ (0.30 g) was subsequently added into the mixture solution and aged for 1 h. Finally, H_2O_2 (10 mL) was added to the mixture under constant stirring to obtain GO sheets.

Synthesis of PB nanoparticles

A 40 mL aqueous solution containing 3.24 g of $FeCl_3\cdot 6H_2O$ and 3.24 g of TSCD was mixed with another 40 mL aqueous solution containing 4.36 g of $Na_4[Fe(CN)_6]\cdot 10H_2O$ and the mixture was vigorously stirred for 1 h before being statically aged overnight to ensure a complete reaction. Finally, the PB nanoparticles were obtained by centrifugation.

Synthesis of GO/IO hybrid materials

The above-prepared GO and PB suspensions were diluted down to 2 mg mL^{-1} by adding water before being mixed together under sonication with specific weight ratios of 25 : 75, 50 : 50, and 75 : 25. The mixtures were continuously treated by sonication for 30 min, and then aged overnight. The GO/PB hybrid precipitates settling at the bottom of the vial were washed with water and ethanol several times, before being dried at room temperature. The GO/IO hybrids were obtained by calcining the GO/PB powders at 400 °C with a heating rate of 1 °C min^{-1}. For comparison, IO and GO samples were obtained by drying up and calcining the PB and the GO suspensions, respectively, under the same conditions.

Characterization

Wide angle X-ray diffraction (XRD) patterns were obtained using Rigaku RINT 2500X with monochromated Cu-Kα radiation (λ = 1.54 Å, 40 kV, 40 mA). Scanning electron microscope (SEM) images were obtained with a Hitachi SU8000 operated at an accelerating of 5 kV. Cross-sectional transmission electron microscope (TEM) and HAADF-STEM (high-angle annular dark-field scanning transmission electron microscope) images were taken with a JEM-2100F operated at an accelerating voltage of 200 kV. Nitrogen (N_2) adsorption–desorption isotherms were measured by Quantachrome Autosorb Automated Gas Sorption System at 77 K. The surface area and pore volume were calculated by the BET and BJH methods, respectively. X-ray photoelectron spectroscopy (XPS) spectra were measured at room temperature using a PHI Quantera SXM (ULVAC-PHI) instrument with an Al-Kα X-ray source.

Electrochemical measurement

The electrochemical measurements were conducted in a three-electrode electrochemical cell with a Pt counter electrode and a Ag/AgCl reference electrode in a 3 M KOH solution. The samples were coated on graphite substrates and used as working electrodes (the graphite substrate serves as a current collector). In detail, the graphite substrates were polished using a fine polisher under constant water flow, etched in a 0.1 M HCl solution at room temperature for 10 min, and finally washed with deionized water in an ultrasonic bath for 30 min. The powder samples were mixed with a poly(vinylidinedifluoride) (20%) in *N*-methyl-2-pyrrolidone (NMP) solvent. The resulting slurries were homogenized by ultrasonication and coated onto the graphite substrates, followed by drying at 80 °C for 2 h in a vacuum oven. Cyclic voltammetry (CV) measurements were obtained using an electrochemical workstation (CHI 660, CH Instruments, USA) in the scan range of 0 to −1.2 V. For every experiment, the typical area under consideration was 1 × 1 cm^2. The specific capacitance value was calculated from cyclic voltammetry using the following equation.

$$C_g = \frac{1}{ms(V_f - V_i)} \int_{V_i}^{V_f} I(V)\mathrm{d}V$$

where C_g is gravimetric capacitance (F g^{-1}), s is the potential scan rate (V s^{-1}), V is the scanned potential within the $V_f - V_i$ window (V), I is current (A), and m is the mass of the active material (g).

3. Result and discussion

The crystal structure and phase purity of the PB nanoparticles were investigated by wide-angle XRD (Fig. 1a). The average crystallite size is calculated to be around 15 nm with the Scherrer equation. This is well-supported by the SEM and TEM images of the synthesized PB nanoparticles which show quasi-spherical shape with an average size of ~15 nm (Fig. S1†). During the synthesis, the surface of both GO sheets and PB nanoparticles were negatively charged. When both suspensions were mixed together, they remained colloidally stable for a certain period. This is critical to maintain a uniform reaction during the preparation of well-organized hybrid materials.

Wide-angle XRD was used to investigate the crystal structure and the phase purity of the products before and after calcination (Fig. 1). The diffraction pattern of the GO sheets displays two peaks at 12° and 26°, which can be assigned to the interlayer spacing between the GO sheets.[17] After hybridization with the PB nanoparticles, the diffraction peaks derived from the GO sheets disappear, while several new intense reflections corresponding to PB can be observed (JCPDF no. 01-070-0557). This indicates that the PB nanoparticles are located within the interlayer spacing of the stacked GO sheets which becomes disordered. The calcination of the GO/PB hybrids with high PB content results in the formation of an impurity-free γ-Fe_2O_3 phase in the resulting hybrid materials, as identified from the XRD peaks at around 35° and 63°. The calcined GO sample shows a sharp diffraction peak at 27° which can be indexed to the peak of stacked GO layers. The peak of stacked GO layers can also be observed in the XRD pattern of the hybrid sample prepared with the GO : PB ratio of 75 : 25, suggesting that there is not enough IO to keep all the GO sheets well-spaced, thus some stacking is still observed.

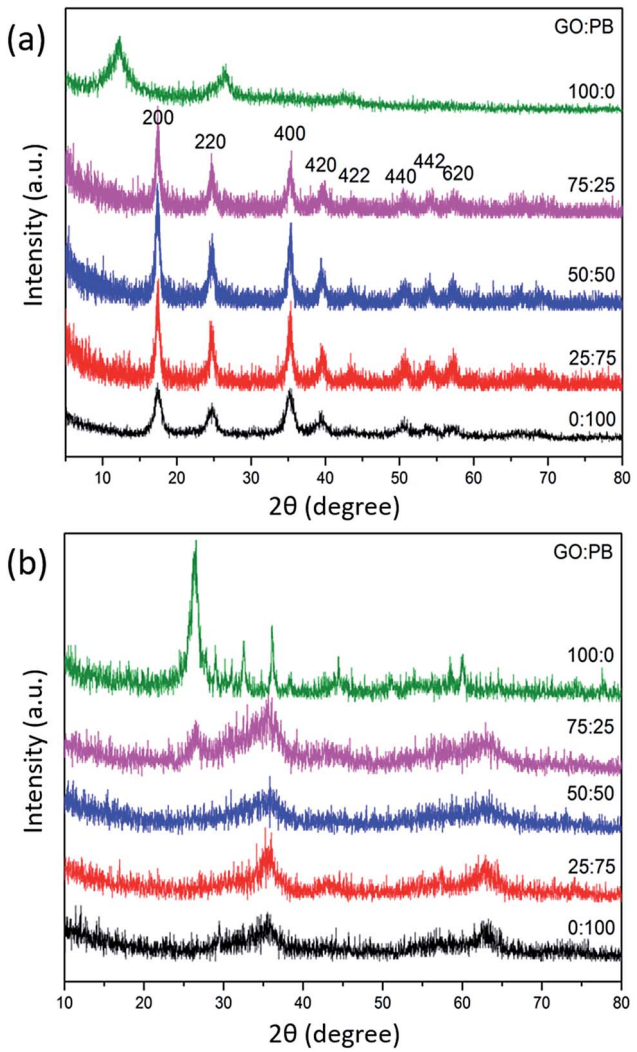

Fig. 1 Wide-angle XRD patterns of samples prepared with various GO : PB ratios (a) before and (b) after calcination.

SEM was utilized to observe the surface morphology of the GO/PB hybrids before and after the calcination (Fig. S2† and 2, respectively). The original 2D morphology of the GO sheets is well-preserved even after calcination. In the case of the GO/IO hybrid samples, the surface of GO is well covered with fine IO nanoparticles, free of aggregates (as observed in the highly-magnified SEM image shown in Fig. S3†) and this observation is supported by the XRD analysis. It can be clearly observed from the cross-sectional HAADF-STEM image and elemental mapping (Fig. S4†) that the IO nanoparticles are well-inserted within the interspaces of the GO sheets. The thicknesses of the GO sheets and the IO layers are around 10–100 nm and 10–60 nm, respectively. High resolution TEM (HRTEM) analysis was employed to investigate the interface between GO and IO (Fig. S5†). The HRTEM image shows lattice fringes with a *d*-spacing of 0.345 nm, which is indexed to the (002) plane of GO. Furthermore, lattice fringes with *d*-spacings of 0.253 nm and 0.295 nm were also observed, which correspond to the (311) and (220) planes of γ-Fe_2O_3, respectively. The obtained hybrid structure containing O, C, and Fe elements were also characterized by XPS, as shown in Fig. S6.†

Upon calcination at high temperatures in air, the C–N bridges in PB were removed to form iron oxides. Our previous study[18] has demonstrated that the result of thermogravimetry/differential thermal analysis/mass spectrometry (TG-DTA-MS) under He/O_2 flow (volume ratio = 80 : 20, flow rate = 200 mL min^{-1}) indicated several exothermic peaks at approximately 260–310 and 470 °C, accompanied with the production of CO_2 and/or N_2O ($m/z = 44$) as well as N_2 and/or CO ($m/z = 28$), which is typical for the combustion reaction of a CN-containing material. In our experiment, we kept the samples at 400 °C for 1 hour during the calcination process, which is enough to completely convert PB into IO and no carbon and nitrogen are identified in the final product. In contrast, under the present calcination temperature (up to 400 °C), the GO is not fully decomposed even in air. Only the decomposition of oxygen-containing groups from the GO sheet is observed at around 170 to 300 °C.[19] It is expected that GO is reduced to rGO during calcination by removal of the functional groups.[20] Therefore, in our calcination process, we can successfully convert the starting GO/PB material to nanoporous rGO/IO hybrid composite.

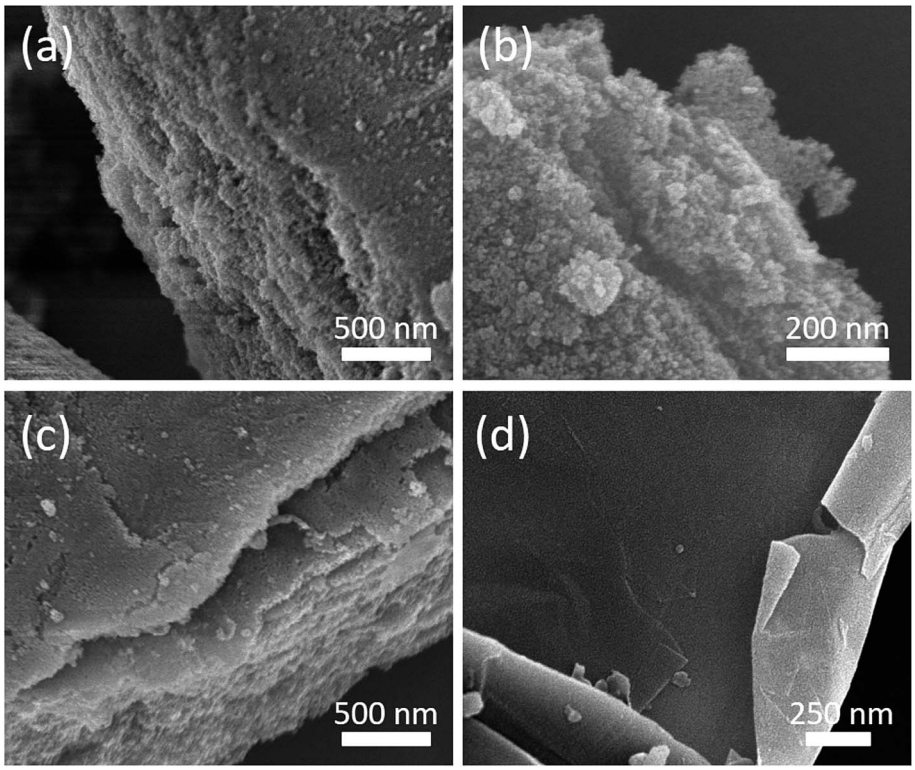

Fig. 2 SEM images of the calcined samples prepared with various GO : PB ratios [the GO : PB ratios are (a) 25 : 75, (b) 50 : 50, (c) 75 : 25, and (d) 100 : 0, respectively].

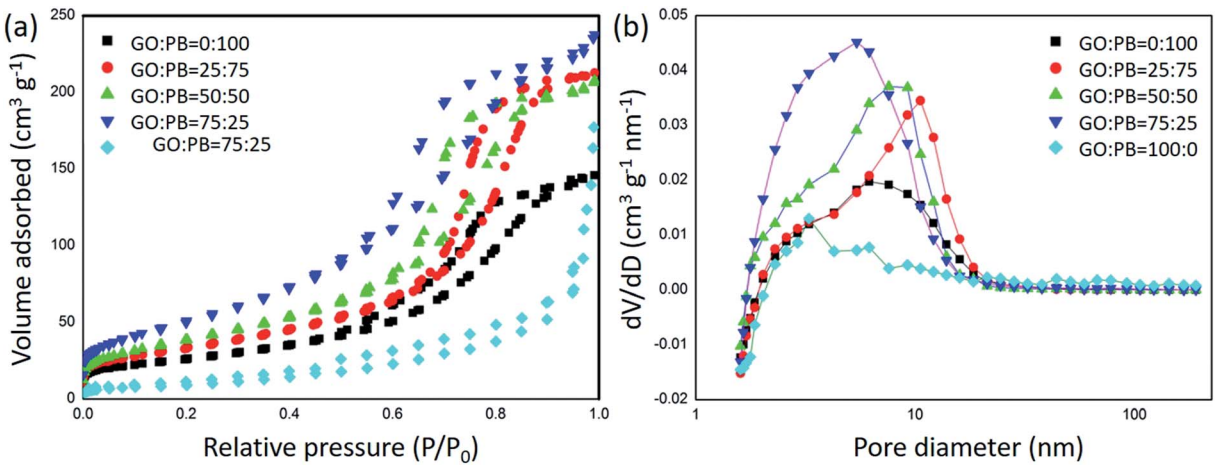

Fig. 3 (a) N_2 adsorption–desorption isotherms of the calcined samples prepared with various GO : PB ratios and (b) their pore size distribution curves obtained by the BJH method.

To evaluate the surface area and porosity the GO/IO hybrids, N_2 adsorption–desorption isotherms were carried out (Fig. 3). The surface areas and the pore volumes were calculated by the BET and BJH methods and the results are summarized in Table 1. While the surface area of IO is larger than that of GO, it is further synergically increased when both materials are combined into one composite. This is expected as the GO sheets offer a much larger available surface when they are appropriately spaced by the IO nanoparticles.

Table 1 Summary of surface area and pore volume of the calcined samples prepared with various GO : PB ratios

GO : PB	Surface area ($m^2\ g^{-1}$)	Pore volume ($cm^3\ g^{-1}$)
100 : 0	34.9	0.228
75 : 25	188.3	0.336
50 : 50	142.6	0.332
25 : 75	120.5	0.384
0 : 100	93.1	0.276

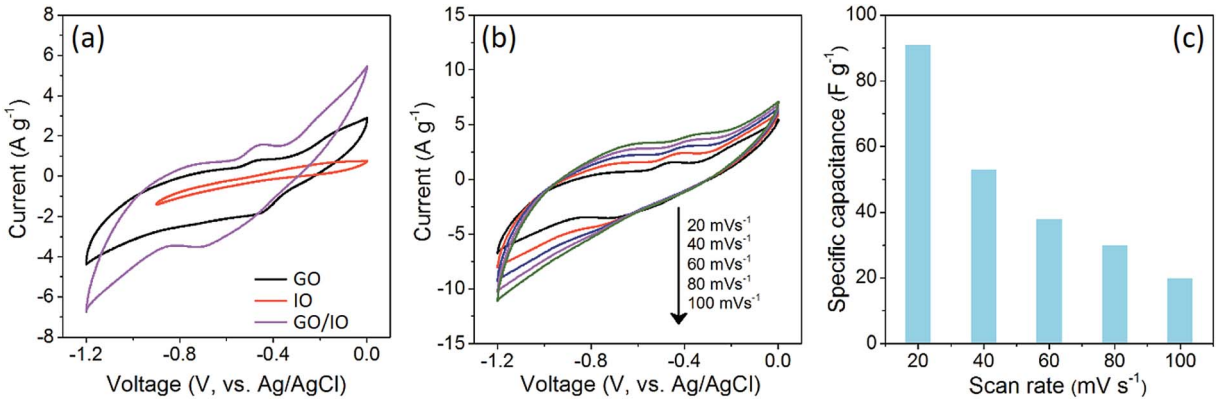

Fig. 4 (a) Comparative CV curves of GO, IO and GO/IO hybrid samples (prepared with GO : PB = 25 : 75), (b) CV curves for GO/IO hybrid sample at the scan rates of 20, 40, 60, 80 and 100 mV s^{-1}, respectively, and (c) variation of specific capacitance with different scan rates for GO/IO hybrid sample.

The rapid growth of portable electronic devices has led to the extensive research into the development of high performance energy storage devices such as supercapacitors and batteries.[21] The electrochemical properties of the synthesized pure GO, pure IO and GO/IO hybrid materials for supercapacitors were studied using a standard three-electrode system. The CV measurements of these three samples (GO, IO, and GO/IO prepared with the GO : PB ratio of 25 : 75) are shown in Fig. 4a. The specific capacitance of the GO/IO hybrid at a scan rate of 20 mV s^{-1} (91 F g^{-1}) is superior to those of the pure components (81 F g^{-1} for GO and 47 F g^{-1} for IO). The GO sheets in the GO/IO composite are well-spaced due to insertion of IO nanoparticles into their interlayer spaces, thus giving the electrolyte easy access to the whole electrode surface, which ultimately results in an improved electrochemical performance, including a higher specific capacitance value. On the other hand, the seriously stacked GO and IO samples show lower surface areas, thus, the ions cannot access the electrode surface effectively. Although IO is a pseudocapacitive material, its resistivity is relatively high and this can hinder its performance for supercapacitor applications. The presence of GO in the GO/IO hybrid can increase the electrical conductivity of the hybrid, whilst also providing a large contact area with the electrolyte, high structural stability, and short transport paths for electrons/ions.

The CV curves of the GO/IO hybrid at various scan rates ranging from 20 to 100 mV s^{-1} are shown in Fig. 4b and c. With increasing scan rates, the capacitance of GO/IO hybrid gradually decreases from 91 F g^{-1} (at 20 mV s^{-1}) to 53 F g^{-1} (at 40 mV s^{-1}), 38 F g^{-1} (at 60 mV s^{-1}), 30 F g^{-1} (at 80 mV s^{-1}), and 20 F g^{-1} (at 100 mV s^{-1}), respectively. At lower scan rates, the pseudocapacitive charge-storage is dominant as implied by the CV shape. As the scan rate increases, however, the oxidation and reduction peaks slightly disappear. This suggests that the EDLC (electric double-layer capacitor) charge storage of the GO component becomes dominant at higher scan rates. More interestingly, our capacitance performance is comparable to the previous literature reports. Our capacitance value is higher than those of FeO_x–carbon nanotubes (84 F g^{-1}),[22] Fe_2O_3 nanorods (64.5 F g^{-1}).[23] Furthermore, though FeOOH nanoparticles have shown a high capacitance of 148 F g^{-1} at 5 mV s^{-1}, they showed a very poor retention performance (44 F g^{-1} at 20 mV s^{-1}).[24] Even though the capacitance value obtained from the present study is not too high, this study still demonstrates the superior electrochemical performance of the GO/IO hybrid compared to the pure GO and IO samples. We believe that our asymmetric supercapacitor (ASC) device development combined with the utilization of other pseudocapacitive materials will further enhance the performance of these cost-effective materials.

4. Conclusions

We have demonstrated the synthesis of a new hybrid material combining GO sheets with PB nanoparticles which was further converted into nanoporous GO/IO composites by thermal treatment in air at 400 °C. The presence of the IO nanoparticles on the GO surface prevents the GO sheets from stacking together, thus leading to a higher surface area. Such an ideal structure gives the electrolyte easy access to the electrode surface, which ultimately results in a higher specific capacitance. Although IO is a pseudocapacitive material, its resistivity is relatively high and this can hinder its performance for supercapacitor applications. The presence of GO in the GO/IO hybrid composite increases the electrical conductivity as well as provides a large contact area with the electrolyte, high structural stability, and short transport paths for electrons. It is expected that by combining GO sheets with other cost-effective and abundant metal oxides such as NiO, Co_3O_4, RuO_2, we can expect a much higher performance in supercapacitors.

Authors contribution

S. T., Y. V. K. and V. M. conceived the idea. S. T., S. M. A. and M. B. Z. carried out the material synthesis. R. R. S., T. A. and S. X. D. carried out the electrochemical testing. Y. V. K. and V. M. were involved in the discussion on the formation mechanism. Y. Y. and M. S. A. H. supervised the project.

Acknowledgements

The authors extend their appreciation to the International Scientific Partnership Program (ISPP) at King Saud University (KSU) for funding this research work through ISPP-0097. Y. V. K., V. M., and M. B. Z. acknowledge the financial support of the Japan Society for the Promotion of Science (JSPS). This study is partially supported by Auto CRC 2020 project 1-111 and DP160102627. The authors would like to thank Dr Macs Bio-Pharma Private Limited for preparation of iron oxide samples.

References

1 (*a*) G. Decher, J. D. Hong and J. Schmitt, *Thin Solid Films*, 1992, **210–211**, 831–835; (*b*) S. S. Shiratori and M. F. Rubner, *Macromolecules*, 2000, **33**, 4213–4219; (*c*) N. Cini, T. Tulun, G. Decher and V. Ball, *J. Am. Chem. Soc.*, 2010, **132**, 8264–8265; (*d*) W. B. Stockton and M. F. Rubner, *Macromolecules*, 1997, **30**, 2717–2725; (*e*) D. J. Schmidt and P. T. Hammond, *Chem. Commun.*, 2010, **46**, 7358–7360; (*f*) V. Kozlovskaya, S. Harbaugh, I. Drachuk, O. Shchepelina, N. Kelley-Loughnane, M. Stone and V. V. Tsukruk, *Soft Matter*, 2011, **7**, 2364–2372; (*g*) H. Lee, L. J. Kepley, H. G. Hong and T. E. Mallouk, *J. Am. Chem. Soc.*, 1988, **110**, 618–620; (*h*) M. Li, S. Ishihara, M. Akada, M. Liao, L. Sang, J. P. Hill, V. Krishnan, Y. Ma and K. Ariga, *J. Am. Chem. Soc.*, 2011, **133**, 7348–7351.

2 W. Tong, X. Song and C. Gao, *Chem. Soc. Rev.*, 2012, **41**, 6103–6124.

3 C. Zhu, S. Guo, Y. Zhai and S. Dong, *Langmuir*, 2010, **26**, 7614–7618.

4 Y. V. Kaneti, J. Moriceau, M. Liu, Y. Yuan, Q. M. Zakaria, X. Jiang and A. Yu, *Sens. Actuators, B*, 2015, **209**, 889–897.

5 D. Yu and L. Dai, *J. Phys. Chem. Lett.*, 2010, **1**, 467–470.

6 D. Chen, H. Feng and J. Li, *Chem. Rev.*, 2012, **112**, 6027–6053.

7 T. Lee, S. H. Min, M. Gu, Y. K. Jung, W. Lee, J. U. Lee, D. G. Seong and B. S. Kim, *Chem. Mater.*, 2015, **27**, 3785–3796.

8 (*a*) R. R. Salunkhe, Y. V. Kaneti, J. Kim, J. H. Kim and Y. Yamauchi, *Acc. Chem. Res.*, 2016, **49**, 2796–2806; (*b*) C. Liu, F. Li, L.-P. Ma and H. M. Cheng, *Adv. Mater.*, 2010, **22**, E28–E62.

9 (*a*) J. Gamby, P. L. Taberna, P. Simon, J. F. Fauvarque and M. Chesneau, *J. Power Sources*, 2001, **101**, 109–116; (*b*) N. C. Abeykoon, J. S. Bonso and J. P. Ferraris, *RSC Adv.*, 2015, **5**, 19865–19873; (*c*) E. Frackowiak and F. Béguin, *Carbon*, 2002, **40**, 1775–1787.

10 Y. B. Tan and J. M. Lee, *J. Mater. Chem. A*, 2013, **1**, 14814–14843.

11 K. T. Nguyen and Y. Zhao, *Nanoscale*, 2014, **6**, 6245–6266.

12 S. G. Kandalkar, D. S. Dhawale, C. K. Kim and C. D. Lokhande, *Synth. Met.*, 2010, **160**, 1299–1302.

13 U. M. Patil, R. R. Salunkhe, K. V. Gurav and C. D. Lokhande, *Appl. Surf. Sci.*, 2008, **255**, 2603–2607.

14 D. P. Dubal, D. S. Dhawale, R. R. Salunkhe, V. S. Jamdade and C. D. Lokhande, *J. Alloys Compd.*, 2010, **492**, 26–30.

15 (*a*) M. Li, F. Pan, E. S. G. Choo, Y. Lv, Y. Chen and J. Xue, *ACS Appl. Mater. Interfaces*, 2016, **8**, 6972–6981; (*b*) A. M. Khattak, H. Yin, Z. A. Ghazi, B. Liang, A. Iqbal, N. A. Khan, Y. Gao, L. Li and Z. Tang, *RSC Adv.*, 2016, **6**, 58994–59000.

16 P. M. Kulal, D. P. Dubal, C. D. Lokhande and V. J. Fulari, *J. Alloys Compd.*, 2011, **509**, 2567–2571.

17 A. Liu and S. Huang, *Sci. China: Phys., Mech. Astron.*, 2012, **55**, 1163–1167.

18 M. B. Zakaria, M. Hu, N. Hayashi, Y. Tsujimoto, S. Ishihara, M. Imura, N. Suzuki, Y. Y. Huang, Y. Sakka, K. Ariga, K. C. W. Wu and Y. Yamauchi, *Eur. J. Inorg. Chem.*, 2014, **2014**, 1137–1141.

19 M. Wojtoniszak, B. Zielinska, R. J. Kalenczuk and E. Mijowska, *Mater. Sci.-Pol.*, 2012, **30**, 32–38.

20 H. Xing, W. Wen and J. M. Wu, *RSC Adv.*, 2016, **6**, 94092–94097.

21 (*a*) R. R. Salunkhe, Y. H. Lee, K. H. Chang, J. M. Li, P. Simon, J. Tang, N. L. Torad, C. C. Hu and Y. Yamauchi, *Chem.–Eur. J.*, 2014, **20**, 13838–13852; (*b*) R. R. Salunkhe, S. H. Hsu, K. C. W. Wu and Y. Yamauchi, *ChemSusChem*, 2014, **7**, 1551–1556.

22 M. B. Sassin, A. N. Mansour, K. A. Pettigrew, D. R. Rolison and J. W. Long, *ACS Nano*, 2010, **4**, 4505–4514.

23 X. Lu, Y. Zeng, M. Yu, T. Zhai, C. Liang, S. Xie, M. S. Balogun and Y. Tong, *Adv. Mater.*, 2014, **26**, 3148–3155.

24 C. Long, L. Jiang, T. Wei, J. Yan and Z. Fan, *J. Mater. Chem. A*, 2014, **2**, 16678–16686.